

Richárd Fiáth, Katharina T. Hofer, Vivien Csikós, Domonkos Horváth, Tibor Nánási, Kinga Tóth, Frederick Pothof, Christian Böhler, Maria Asplund, Patrick Ruther and István Ulbert*

Long-term recording performance and biocompatibility of chronically implanted cylindrically-shaped, polymer-based neural interfaces

<https://doi.org/10.1515/bmt-2017-0154>

Received August 30, 2017; accepted November 20, 2017

Abstract: Stereo-electroencephalography depth electrodes, regularly implanted into drug-resistant patients with focal epilepsy to localize the epileptic focus, have a low channel count (6–12 macro- or microelectrodes), limited spatial resolution (0.5–1 cm) and large contact area of the recording sites (~mm²). Thus, they are not suited for high-density local field potential and multi-unit recordings. In this paper, we evaluated the long-term electrophysiological recording performance and histocompatibility of a neural interface consisting of 32 microelectrodes providing a physical shape similar to clinical devices. The cylindrically-shaped depth probes made of polyimide (PI) were chronically implanted for 13 weeks into the brain of rats, while cortical or thalamic activity (local field potentials, single-unit and multi-unit activity) was recorded regularly to monitor the temporal change of several features of the electrophysiological performance. To examine the tissue reaction around the probe, neuron-selective and astroglia-selective immunostaining methods were applied. Stable single-unit and multi-unit activity were recorded for several weeks with the implanted depth probes and a weak or moderate tissue reaction was found around the probe track. Our data on biocompatibility

presented here and *in vivo* experiments in non-human primates provide a strong indication that this type of neural probe can be applied in stereo-electroencephalography recordings of up to 2 weeks in humans targeting the localization of epileptic foci providing an increased spatial resolution and the ability to monitor local field potentials and neuronal spiking activity.

Keywords: depth probe; electrophysiological performance; histocompatibility; multielectrode recording; single-unit activity; stereo-electroencephalography.

Introduction

Recording electrical activity from the brain provides invaluable information regarding the mechanisms underlying basic and higher order brain functions. Intracortical electrophysiological recording methods are common practice in animal experiments; however, in humans, invasive electrophysiology is largely limited due to strict ethical restrictions and the lack of appropriate apparatus for high-density neural recordings [1]. Furthermore, most of the electrophysiological recording devices developed for clinical use or for acute/semichronic recordings in

***Corresponding author: István Ulbert,** Institute of Cognitive Neuroscience and Psychology, Research Centre for Natural Sciences, Hungarian Academy of Sciences, Magyar tudósok körútja 2, H-1117 Budapest, Hungary, Phone: +36-1-382-6801, Fax: +36-1-382-6295, E-mail: ulbert.istvan@ttk.mta.hu; and Faculty of Information Technology and Bionics, Pázmány Péter Catholic University, H-1083 Budapest, Hungary

Richárd Fiáth: Institute of Cognitive Neuroscience and Psychology, Research Centre for Natural Sciences, Hungarian Academy of Sciences, H-1117 Budapest, Hungary; and Faculty of Information Technology and Bionics, Pázmány Péter Catholic University, H-1083 Budapest, Hungary

Katharina T. Hofer and Vivien Csikós: Faculty of Information Technology and Bionics, Pázmány Péter Catholic University, H-1083 Budapest, Hungary

Domonkos Horváth: Institute of Cognitive Neuroscience and Psychology, Research Centre for Natural Sciences, Hungarian Academy of Sciences, H-1117 Budapest, Hungary; Faculty of

Information Technology and Bionics, Pázmány Péter Catholic University, H-1083 Budapest, Hungary; and School of Ph.D. Studies, Semmelweis University, H-1085 Budapest, Hungary

Tibor Nánási and Kinga Tóth: Institute of Cognitive Neuroscience and Psychology, Research Centre for Natural Sciences, Hungarian Academy of Sciences, H-1117 Budapest, Hungary

Frederick Pothof: Microsystem Materials Laboratory, Department of Microsystems Engineering (IMTEK), University of Freiburg, D-79110 Freiburg, Germany

Christian Böhler and Maria Asplund: Electroactive Coatings Group, Department of Microsystems Engineering (IMTEK), University of Freiburg, D-79110 Freiburg, Germany; and BrainLinks-BrainTools Cluster of Excellence at the University of Freiburg, D-79110 Freiburg, Germany

Patrick Ruther: Microsystem Materials Laboratory, Department of Microsystems Engineering (IMTEK), University of Freiburg, D-79110 Freiburg, Germany; and BrainLinks-BrainTools Cluster of Excellence at the University of Freiburg, D-79110 Freiburg, Germany

patients with neurological disorders (e.g. epilepsy, Parkinson's disease) contain only a small number of macro- and microelectrodes [2–7]. Thus, these implantable neural probes (e.g. stereo-electroencephalography depth electrodes) offer only low spatial resolution and are inadequate to monitor the spiking activity of many individual neurons simultaneously. Therefore, to maximally exploit the potential of human intracortical recordings, the development and use of novel, high-channel-count recording devices are necessary. Neural probes designed for long-term monitoring of human brain electrical activity have to be made of biocompatible materials and should consist of a high number of microelectrodes capable of recording local field potentials, multi-unit and single-unit activity (MUA and SUA, respectively) simultaneously to obtain as much useful data as possible during the rare opportunities of recording from the brains of patients.

The technology to realize high-density electrophysiological recording devices is readily available [8, 9], however, prior to the application of these novel depth probes in human patients, thorough validation experiments in animal models are required. This includes the long-term testing of the recording performance of the neural implants and the examination of the foreign body response of the brain tissue in the vicinity of the depth probe [10, 11]. In a recent study, we have developed the prototype of a high-channel-count, cylindrically-shaped probe made of polyimide (PI) [8]. The functionality of the probes was verified by chronically implanting them for several weeks into the brain of a rhesus monkey [9].

Parallel to the monkey experiments, another probe variant had been developed. The main purpose of this probe type is to evaluate tissue reactions based on histological data, which in the case of rhesus monkeys is very limited, due to the fact that the probe was only implanted in one monkey. This paper presents the chronic evaluation of this cylindrically-shaped hollow depth probe realized from PI-based thin-film substrates containing 32 microelectrodes around the circumference of the probe cylinder. To assess the electrophysiological performance and histocompatibility of the fabricated neural interfaces, we implanted them chronically into the neocortex or thalamus of rats for a period of about 3 months. The temporal evolution of the recording performance was investigated by tracking changes in the number of separable single units, the signal-to-noise ratio (SNR) of recorded neural data and the electrical impedance of recording sites. Finally, the depth probes were explanted after the chronic implantation period and immunohistochemical methods were used to examine the loss of neurons and

the glial reaction adjacent to the track of the cylindrical depth probe.

Materials and methods

Probe design and fabrication

The probe fabrication was described in detail previously [8, 9]. In short, dual-layer lift-off technique was employed to pattern metal traces (Figure 1B) on top of a PI substrate (U-Varnish-S, UBE Industries Ltd., Tokyo, Japan) spin-coated and cured on a 100 mm silicon wafer (Figure 1A). Subsequently, a second PI layer and an additional Cytop® layer (Asahi Glass Co., Tokyo, Japan) were spin-coated to embed the metal tracks and electrodes in the insulating polymer layers (Figure 1C). This was followed by photolithography to generate soft etch masks for the reactive ion etching steps used to define the lateral dimensions of Cytop® (Figure 1D), openings to the electrodes and contact pads and probe dimensions (Figure 1E). The PI foil was peeled off the silicon wafer using tweezers (Figure 1F) and finally rolled into the cylindrical probe shape inside a metallic mold with an inner diameter of 800 µm using customized tools (Figure 2A–D). The probe substrate inside the mold was heated to a temperature of 290°C which exceeds the glass-transition temperature of Cytop®. Providing enough time, i.e. 4 h in our case, allowed to adhesively bond the overlapping PI surfaces and thus to maintain the cylindrical probe shape after removing the probe from the mold.

The cylindrical depth probe was electrically interconnected to the electrophysiological recording setup via a planar section of the PI structure which could be attached to a zero-insertion-force (ZIF) connector (Molex, Lisle, IL, USA; Figure 2E). To avoid the mechanical failure of the PI foil due to the frequent usage of the ZIF connector during experiments lasting several weeks, the PI structure was connected to a small and flexible printed circuit board, as described in the work of Pothof et al. [9].

The hollow depth probe developed in this study is schematically shown in panel A of Figure 3. The PI-based neural implant has

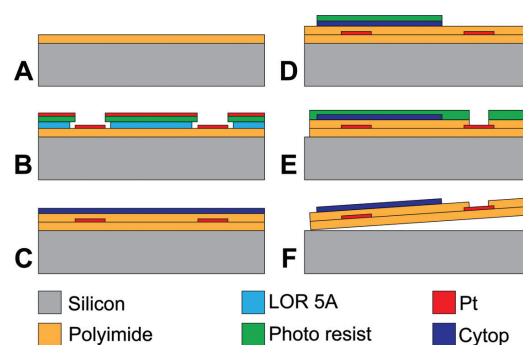


Figure 1: Schematic of cleanroom processing steps.

(A) Spin coating the first PI layer; (B) lift-off patterning of metal tracks and electrodes; (C) embedding metal tracks into insulating polymers; patterning of (D) Cytop® and (E) PI layers to define adhesive layer and probe dimensions by reactive ion etching, respectively; (F) peeling off finalized probe substrates from the silicon handle wafer.

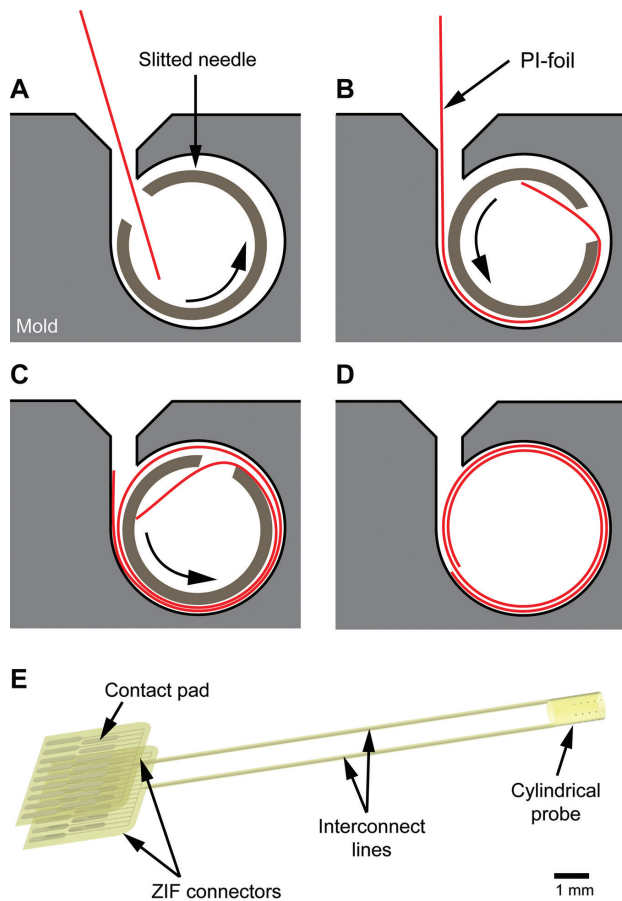


Figure 2: Schematic cross-section of the rolling process. (A) PI-based probe substrate (red) tangentially introduced through the slits of the metallic mold and a slitted needle. (B, C) Rotation of the needle to completely drag the PI foil into the mold after two full revolutions. (D) Axial needle retraction and thermal anneal of the cylindrical probe inside the mold cavity at elevated temperatures. (E) Schematic image of the device showing the planar ZIF connector extending from the cylindrical probe.

a cylindrical shape (height: 1500 μm , diameter: 800 μm) with 32 integrated platinum (Pt) microelectrodes having a diameter of 35 μm . The electrodes are arranged on the PI substrate in four rows with a distance of 200 μm . The rows are transferred in the cylindrically-shaped probe into respective rings in each of which the eight recording sites are positioned equidistantly around the circumference of the probe cylinder (Figure 3A). The adjacent rings of electrodes are 200 μm apart from each other, with the first ring of electrodes being located 100 μm away from the bottom edge of the probe. Panel B in Figure 3 shows an optical micrograph of a probe cylinder realized using the as described process sequence. The micrograph illustrates the metal tracks to interface the individual electrodes.

In a subset of probes ($n=3$), nanostructured platinum coating (Pt-nanograss) was deposited on the surface of all the microelectrodes with the aim of reducing their electrical impedance and, as a consequence, to increase the SNR of neural recordings. The deposition process is described in detail in Boehler et al. [12]. Measured at 1 kHz, regular Pt electrodes showed electrical impedance values in the range of 200–400 k Ω [8, 9], while an impedance decrease of more

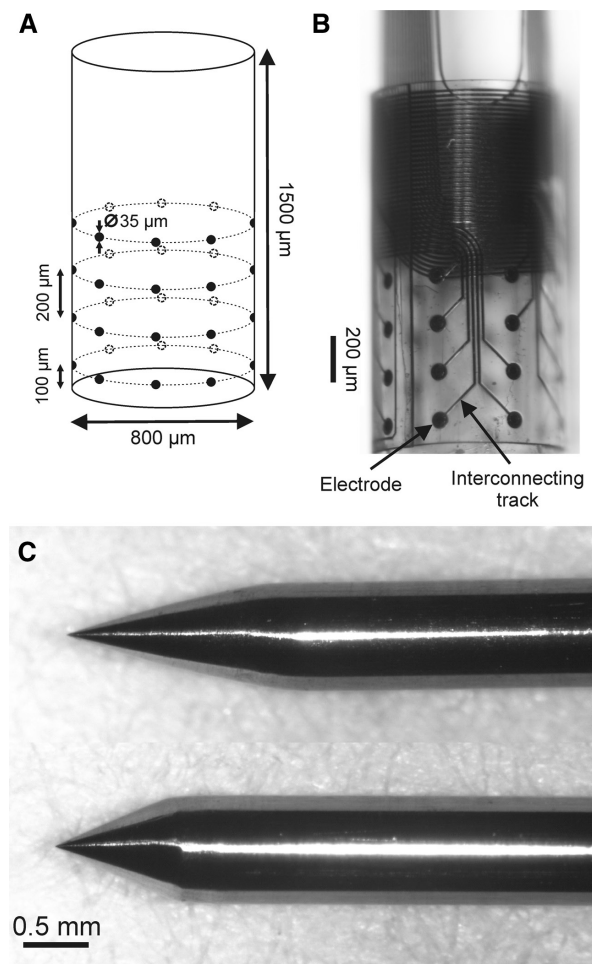


Figure 3: Dimensions and physical appearance of the neural implant assembled for chronic implantation.

(A) Schematic representation and (B) optical micrograph of the cylindrical probe with 32 microelectrodes. (C) The two types of stainless steel wires with different tip angles used to aid the penetration of the probe into the brain tissue during implantation.

than one order of magnitude could be achieved after the deposition of the nanograss coating (~ 20 k Ω , [12]).

Preparation of the neural interface for chronic implantation

Stainless steel wires with a diameter of 800 μm were used to facilitate the implantation procedure (Figure 3C). The tip of each wire was sharpened to form a cone with an opening angle of either 40° or 60°. These wires were pushed through the opening of the hollow probe body until their tips were located 1–2 mm below the bottom of the probe. After that, the wires were carefully fixed to the probe with the aid of two-component epoxy resin (EPO-TEK 301-2, John P. Kummer GmbH, Augsburg, Germany). After the cure time (48 h at room temperature), the probe was attached to a motorized microdrive (Robot Stereotaxic – StereoDrive, Neurostar GmbH, Tübingen, Germany), and sterilized before implantation by immersing it in 70% ethanol for

5 min, followed by washing it with a continuous stream of distilled water for 2 min.

Surgical implantation procedure

Nine Wistar rats (weight: 423 ± 41 g, range: 350–500 g, adult males) were used for the chronic experiments. All experiments were performed according to the EC Council Directive of November 24, 1986 (86/89/EEC), and all procedures were reviewed and approved by the local Ethical Committee and the National Food Chain Safety Office of Hungary (license number: PEI/001/2290-11/2015). Animals were anesthetized with a mixture of ketamine (375 mg/ml) and xylazine (5 mg/ml) injected intramuscularly at 2 ml/kg body weight injection volume. If necessary, supplementary ketamine/xylazine injections were given (0.3 ml/h) to maintain the depth of anesthesia during surgery. After the rats reached the level of surgical anesthesia, they were placed in a stereotaxic frame (David Kopf Instruments, Tujunga, CA, USA). Their body temperature was maintained with a homeothermic heating pad connected to a temperature controller (Supertech, Pécs, Hungary). First, the skull was exposed by a small incision which was followed by the removal of the connective tissue between the skin and the skull using a bone scraper. Subsequently, the skull of the animal was cleaned with a 4% solution of hydrogen peroxide. Following that, a small amount of dental etching gel containing 38% phosphoric acid (Etch-Rite, PULPDENT Corporation, Watertown, MA, USA) was used on top of the skull to increase the surface area for a better adhesion of the dental acrylic applied later during the surgery. Five small screws with a diameter of 0.9 mm were mounted on the skull to stabilize the implant. One of the screws which was driven into the skull over the cerebellum served as the reference and ground electrode during the recordings.

A 3×3 mm² craniotomy was drilled over the trunk region of the primary somatosensory cortex (S1Tr, $n = 3$ rats, craniotomy: anterior-posterior (AP): -1.5 mm to -4.5 mm, medial-lateral (ML): 1.5 mm to 4.5 mm, with respect to the bregma [13]) for cortical recordings [dorsal-ventral (DV) depth: -1 – 2 mm], or over the parietal association cortex (PtA, $n = 6$ rats, craniotomy: AP: -1.5 mm to -4.5 mm, ML: 2 mm to 5 mm, with respect to the bregma) to target the ventrobasal complex in the thalamus (DV depth: -5 – 7 mm). The dura mater was carefully removed before the implantation with the aid of a 30-gauge needle. Care was taken to avoid damaging large blood vessels during the removal of the dura and during probe implantation. Room temperature physiological saline solution was dripped into the cavity of the craniotomy to prevent dehydration of the cortex. Furthermore, to prevent the eyes of the animal from drying during surgery, paraffin oil (Hunгарopharma, Budapest, Hungary) was regularly dropped onto them.

After the removal of the dura mater, the probe was advanced slowly with an insertion speed of 2 – 3 μ m/s to the appropriate brain depth corresponding to the target location (Neocortex: S1Tr, AP: -2.5 mm, ML: 2.5 mm; Thalamus: ventral posterolateral and ventral posteromedial nuclei (VPL/VPM), AP: -3.5 mm, ML: 3 mm, with respect to the bregma [13]) using a motorized microdrive and the guidance of a surgical microscope.

Self-polymerizing methyl methacrylate (Self-Curing Denture Repair Material, Vertex-Dental, Zeist, The Netherlands) was applied to cement the probe and screws to the skull. Before the application, a small piece of sterile gelatin sponge (Gelaspon, Germed, Rudolstadt, Germany) was placed carefully on top of the cortex around

Table 1: The targeted anatomical region and the electrode material of the cylindrical probe for each implanted animal.

Animal number	Brain region	Electrode material
1	Thalamus	Regular Pt
2	Thalamus	Regular Pt
3	Neocortex	Regular Pt
4	Thalamus	Pt-nanograss
5	Thalamus	Pt-nanograss
6	Neocortex	Regular Pt
7	Thalamus	Regular Pt
8	Neocortex	Pt-nanograss
9	Thalamus	Pt-nanograss

the implant to protect the brain from direct contact with the dental acrylic. A small, bowl-like structure was formed from acrylic on top of the cemented region to serve as a protective shield around the connectors of the implant. Finally, several sutures were placed to stabilize the skin around the acrylic structure, and the head wound was sterilized with Betadine (Egis Pharmaceuticals PLC, Budapest, Hungary). Table 1 shows the targeted anatomical region and the electrode material of the cylindrical probe for each implanted animal.

Electrophysiological recording sessions

Brain electrical activity was measured in a Faraday cage on a regular basis, usually every 2 or 3 days. Animals had unlimited access to food and water between the recording sessions. Before recording, the rats were temporally sedated using a small dose (~ 0.8 ml) of isoflurane (Isofluran CP, Medicus Partner, Biatorbágy, Hungary). This was followed by the intramuscular administration of a small amount (0.3 ml) of ketamine/xylazine mixture, with the same proportion of ingredients as used during the implantation, to induce light anesthesia. Before attaching the recording setup to the connectors located on the head of the animal, the area around the acrylic cap was cleaned with a sterile cotton bud and treated with Betadine to avoid infections. Each recording session lasted about half an hour. At the end of each recording session, the electrical impedance of the recording sites was measured at 1 kHz (for further details see the “Impedance measurement and analysis” section).

Data acquisition

Brain signals were recorded using an Intan RHD2000 electrophysiological recording system (Intan Technologies LLC., Los Angeles, CA, USA) comprising a 32-channel headstage. The recording system was connected to a laptop via USB 2.0. Wideband signals (0.1–7500 Hz) were recorded with a sampling frequency of 20 kHz and a resolution of 16 bit. Data files containing 5-min-long continuous recordings were saved to the hard drive of the laptop for offline data analysis.

Histology

After 13 weeks, the animals were deeply anesthetized with a high dose of ketamine/xylazine cocktail and transcardially perfused with

physiological saline (100 ml) followed by a fixative containing 4% paraformaldehyde and 15% picric acid in 0.1 M phosphate buffer (PB, 250 ml). The stainless steel wire with the probe attached was carefully pulled out from the brain tissue by hand under microscopic inspection, then the fixed brain was removed from the skull and stored at 4 °C overnight in the fixative solution. No brain tissue residue was observed on the electrode by microscopic inspection. After that, 60-µm-thick horizontal sections were cut with a vibratome (Leica VT1200S, Leica Microsystems GmbH, Wetzlar, Germany) from brain areas containing the probe tracks. Care was taken to process only those sections which were located in the depth of the recording probe, but not those which contained the track of the stainless steel wire. The selection of appropriate sections was achieved in the following way. The depth of the implantation was known, as well as the length of the protruding section of the stainless steel wire, and the length of the cylindrical probe. Based on this information, we could estimate the position of the probe cylinder in the brain tissue. Then, we started to cut 60-µm-thick brain sections starting from the dorsal side of the brain (top of the neocortex), which corresponds to a depth of 0 µm. When the depth indicator of the vibratome reached the appropriate depth (i.e. the level of the first row of recording sites), brain slices (~10) selected for immunostaining were moved to PB until we reached the depth corresponding to the bottom side of the cylinder.

In short, the immunostaining protocol of the brain tissue was as follows. After washing in 0.1 M PB, the sections were immersed in 30% sucrose for 1–2 days, and then freeze-thawed three times over liquid nitrogen, and washed in 0.1 M PB. The endogenous peroxidase activity was blocked by 1% H₂O₂ in Tris-buffered saline (TBS, 10 min). The non-specific immunoglobulin binding of the tissue was blocked by 2% normal goat serum (Vector Laboratories, Burlingame, CA, USA) and 2% normal horse serum (Vector Laboratories) in TBS (45 min). For the visualization of neurons and glial cells, a monoclonal mouse antibody against neuronal nuclei (NeuN, EMD Millipore, Billerica, MA, USA, 1:2000) and a monoclonal mouse antibody against glial fibrillary acidic protein (GFAP, EMD Millipore, 1:2000) were used, respectively. For the visualization of immunopositive elements, biotinylated anti-mouse immunoglobulin G (Vector Laboratories) was applied as secondary serum (1:250, 2 h) followed by avidin-biotinylated horseradish peroxidase complex (Vector Laboratories, 1:250, 1.5 h). The sections were preincubated in 3,3'-diaminobenzidine-tetrahydrochloride hydrate chromogen (DAB, 0.05 %, dissolved in Tris buffer, 20 min) and then developed by 0.01% H₂O₂. After washing in Tris buffer and PB, sections were mounted, dehydrated for light microscopy (2×10 min in xylene) and coverslipped with DePex (Serva Electrophoresis GmbH, Heidelberg, Germany). The stained sections were photographed under a light microscope (Leica DM2500, Leica Microsystems GmbH).

Data analysis

The NeuroScan Edit 4.5 (Compumedics, Charlotte, NC, USA) software and custom software written either in MATLAB (MathWorks Inc., Natick, MA, USA) or in C++ were used for offline signal processing and analysis.

Spike sorting: Spike sorting was performed separately on at least three data files obtained during each recording session. The isolation of the activity of single units was accomplished in a similar way

as described in Fiath et al. [14]. In short, the continuous, wideband signals were digitally band-pass filtered (500–5000 Hz, zero-phase shift, 24 dB/octave) to remove local field potentials. Spikes were then detected using a threshold of >5 times the standard deviation (SD) from the mean of the root mean square (RMS) of the filtered traces computed in a sliding window (0.2 ms) [15]. Following that, the extracted spike waveforms were aligned to their negative peaks and the first three principal components were calculated on each of the channels for each of the detected action potentials. Finally, single units were identified and isolated manually with the aid of a cluster cutting software (Klusters; [16]). Autocorrelograms of the units were checked for clear refractory periods (no spikes in the range of 0–3 ms), which was one of our criteria for good unit isolation. Another criterion was that the majority of points corresponding to the separated neuron cluster were clearly segregated from the rest of the points on at least one of the planes of the waveform parameters (principal components) displayed by Klusters.

Calculation of the signal-to-noise ratio: The SNR of cortical and thalamic recordings was calculated using the MATLAB implementation of the adaptive-threshold spike detection method (STH) described in Seidl et al. [17]. First, the wideband data were band-pass filtered (500–5000 Hz, zero-phase shift, 24 dB/octave) to obtain the unit activity. After that, we applied the STH method on the filtered traces to detect spikes for the calculation of the signal power. A 30-s-long section of the recordings was used to compute the SNR with the following formula:

$$\text{SNR}_{\text{dB}} = 20 \cdot \log_{10} \frac{\frac{1}{N} \sum_{n=1}^N \text{RMS}(\text{spike}_n(t))}{\hat{\sigma}_{\text{noise}}},$$

where $\text{RMS}(\text{spike}_n(t))$ is a quality measure of the individual spike and denotes the root mean square of spike n measured in a 1-ms-long window centered around the spike detected with the STH method [17]. The noise ($\hat{\sigma}_{\text{noise}}$) is the estimate of the noise SD calculated by the RMS of all mean centered values outside the spike windows which are the pure noise segments [17]. Traces containing large (>1 mV) artifacts or high-frequency noise contaminating the unit activity were excluded from the analysis. The SNR was computed on all channels, followed by the calculation of the mean and SD of the SNR across channels. Furthermore, in the case of two experiments, channels were grouped into one of the following three categories based on their SNR values: high SNR ($\text{SNR} \geq 3.5$ dB), moderate SNR ($3.5 \text{ dB} > \text{SNR} \geq 1.5$ dB), low SNR ($\text{SNR} < 1.5$ dB). Finally, to examine the temporal change of the SNR across weeks, the grand average SNR was computed and visualized.

Impedance measurement and analysis: During each recording session, the electrical impedance of the recording sites was measured in the brain at 1 kHz frequency against the stainless steel screw electrode located over the cerebellum which served as a combined ground and reference electrode. Impedance measurements were performed using the built-in feature of the electrophysiological recording system (Intan RHD2000 evaluation system) which has on-chip circuitry to generate an AC current waveform needed to measure electrical impedance of the recording sites. Only the impedance values of the six probes implanted for 13 weeks (three probes with regular Pt electrodes and three probes with Pt-nanograss recording sites) were used in further calculations. Electrodes with high impedance values

(>10 M Ω , probably accidentally covered with epoxy resin) or unable to record physiologically meaningful data (e.g. due to shorted electrodes or wire breaks) were removed from further calculations. To assess the impedance changes over time, first, we averaged the electrical impedance values measured for all recording sites of probes with a specific electrode coating during a single recording session. Then, in case there were multiple impedance measurements during a 7-day period, the mean impedance values corresponding to these recording sessions were averaged. Finally, for both probe types (comprising either Pt electrodes or electrodes covered by Pt-nanograss), we calculated the grand average impedance for each week.

Evaluation of immunostained sections: The loss of neurons and the level of astroglial reaction was investigated post-mortem around the probe track using the immunostained histology sections. Out of the nine implanted animals, sections from six animals surviving the 3 months were included in this analysis. For each animal, three GFAP- and three NeuN-stained sections were selected for the histological analysis. Sections from animals with thalamic ($n=4$; DV depth: ~5–7 mm) and neocortical ($n=2$; DV depth: ~1–2 mm) implants were analyzed separately.

The NeuN-stained sections were analyzed as follows. Automatic cell detection was carried out by a custom MATLAB script. The approach used here exploits the fact that cell nuclei are intensively marked by the NeuN staining. First, the input image was inverted, so the brightness levels became proportional to NeuN staining intensity. Then, the inverted image was converted to grayscale (“IG”), with levels normalized between 0 (black) and 1 (white). From this, a smoothed image was produced using MATLAB’s “imfilter” function (“IGS”), employing an average filter created by “fspecial” with a size of 25 pixels (26.7 μm). Subtracting “IGS” from “IG” yields to an adaptive thresholded differential image (“AI”). Areas of “AI” with values greater than a heuristic threshold (0.1) were accepted as putative cell nuclei regions and converted to a binary mask (“BI”). As a second step, the grayscale image (“IG”) was multiplied by the binary mask (“BI”) to get an intensity image of the putative cell nuclei regions with removed background. Using a Gaussian filter of a size of 9 pixels (9.6 μm), local noise was smoothed out on this image, then, regional maxima were localized. Those maxima were accepted as the positions of the auto-detected cell nuclei. After detection of neurons, the outline of the probe track was defined manually for each section. Areas comprising strongly varying cell densities for anatomical reasons were excluded from the analysis. For each identified neuron and pixel, the minimal distance to the probe track was determined. Next, regions of interest (ROIs) were defined around the clearly visible probe track. The first ROI included the pixels that are not more than 25 μm away from the track edge. The next ROI included pixels that are more than 25 and not more than 50 μm away from the probe edge. In total, 20 such ROIs were defined, so that the last ROI included pixels that are more than 475 and less than 500 μm away from the track edge. For each ROI, the cell density (cells per μm^2) was calculated and expressed as a percentage (i.e. standardized) compared to the average cell density in the ROIs from 400 to 500 μm , which served as a control.

The photographs of the GFAP sections were analyzed using Fiji [18, 19] and MATLAB. First, the images were converted to grayscale and then an automatic threshold was applied to detect black pixels indicating stained glial cells that form a glial scar around the probe track. ROIs were defined as described for the NeuN sections above. Then, thresholded black pixels, along with the total number of pixels in each ROI, were counted automatically in MATLAB. The relative

number of black pixels in each ROI was computed as the number of black pixels in the ROI divided by the number of all pixels in the same ROI. These numbers were standardized to the mean in the ROIs from 400 to 500 μm .

Both for the NeuN and the GFAP analysis, Kruskal-Wallis tests were performed, comparing the standardized cell densities or black pixel numbers in the 20 analyzed ROIs. Separate tests were performed for the neocortex and thalamus. *Post-hoc* analysis comparing average group ranks was performed for significant Kruskal-Wallis tests results. *p*-Values <0.05 were considered significant.

Results

General recording characteristics

Cylindrically-shaped, PI-based neural interfaces with 32 microelectrodes (Figure 3A and B) were chronically implanted into the neocortex or thalamus of rats for 13 weeks (Table 1). As the probes had a relatively large diameter (800 μm) and a blunt end, they were attached to stainless steel wires with sharp tips (Figure 3C) to facilitate the insertion into the brain tissue and to reduce brain dimpling during implantation. Three animals out of nine were removed earlier from the study due to health complications (after 1, 2 and 5 weeks, respectively). The remaining six animals were sacrificed after 3 months for the histological examination of the brain tissue.

To characterize the recording capabilities of the implanted probes, we monitored the wideband (0.1–7500 Hz) brain electrical activity on a regular basis and analyzed the single-unit and multi-unit activity, i.e. the spiking activity of neurons located close to the microelectrodes. In general, wideband activity, which contains both local field potentials (0.1–500 Hz) and unit activity (500–5000 Hz), could be recorded with good quality during the first weeks after implantation, both from the neocortex and thalamus of several rats (Figure 4A and B). Recordings were done in light ketamine/xylazine anesthesia during which up-states (with high unit activity) and down-states (with ceased action potential firing), the hallmarks of the rhythmic slow-wave activity, could be observed in both brain structures (Figure 4A and B; [20]).

Well-separable single units with stable firing patterns and with peak-to-peak action potential amplitudes over 100 μV have been detected on several channels (Figure 4C and D), suggesting that at least some of the neurons close to the depth probe survived the implantation. Both bursting (multiple spikes fired in rapid succession) and non-bursting neurons appeared on the recordings. Bursting single units were present mostly in the thalamus (e.g. Figure 4D), where the burst mode is the dominant

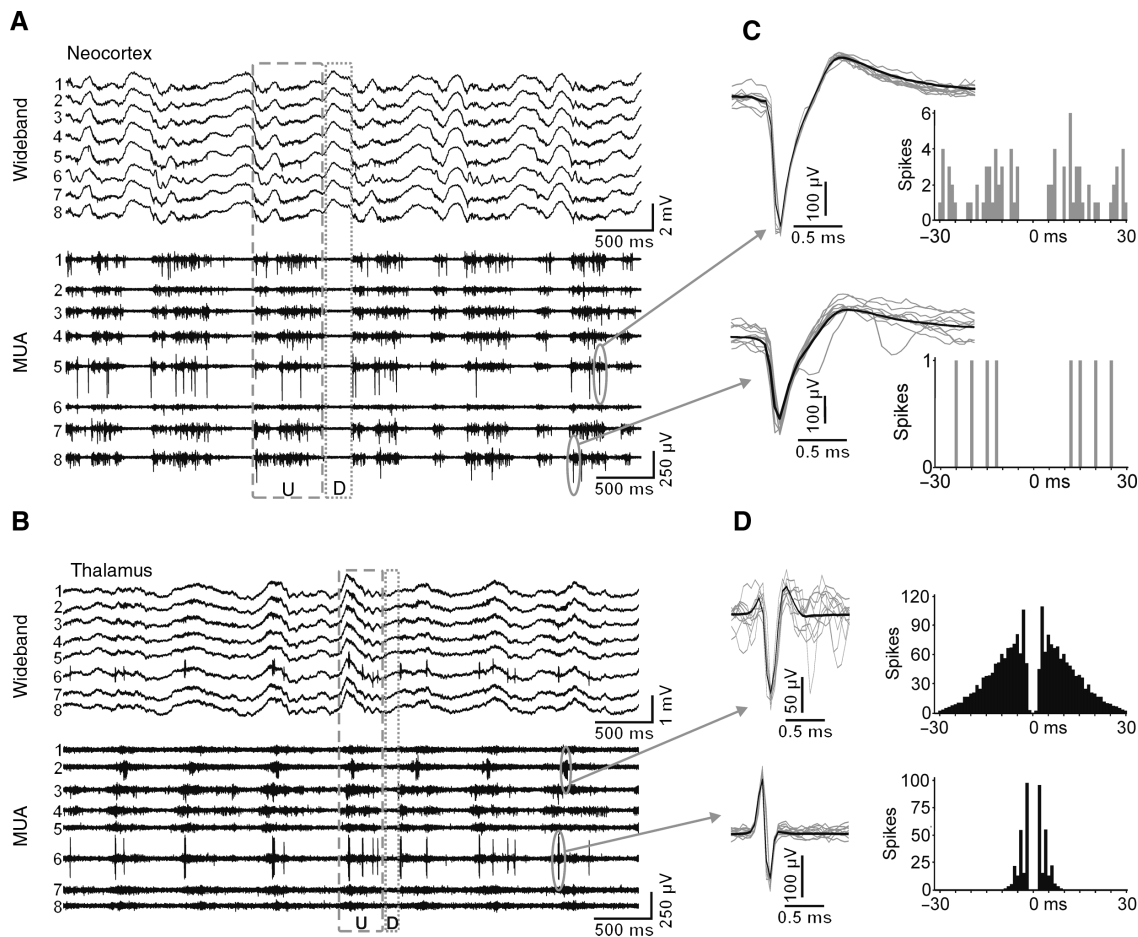


Figure 4: Brain electrical activity obtained with cylindrical probes from anesthetized rats. Representative 5-s-long traces of wideband (0.1–7500 Hz) and multi-unit activity (MUA, 500–5000 Hz) recorded on eight channels of probes implanted in the neocortex (A) and in the thalamus (B). Sample up-states (“U”, high spiking activity) and down-states (“D”, ceased action potential firing) are indicated by dashed and dotted boxes, respectively. (C, D) Examples of cortical (C) and thalamic (D) spike waveforms of single units after spike sorting. Demonstrated neurons were selected from recordings presented in panel A and B (gray arrows). Ten single spikes (waveforms in gray color) and the mean spike waveform (black waveform) of single units are shown. The autocorrelogram of neurons (bin size: 1 ms) is displayed next to the waveforms, on the right hand side.

firing pattern under ketamine/xylazine anesthesia [21]. In some cases, we could record the activity of a dozen or more single units simultaneously. Furthermore, in thalamic recordings, we could observe the propagation of the MUA during up-states around the circumference of the probe cylinder (Figure 5). In one of our previous studies where we used high-density silicon probes for the electrophysiological recordings, we detected similar propagating activity patterns in the thalamus of rats under ketamine/xylazine anesthesia [14].

Long-term electrophysiological performance

Single-unit or multi-unit activity could be detected in all animals about two hours after implantation; however,

the quality of the recorded unit activity was variable over time and across animals. Generally, the number of separable single units peaked during the first 2 weeks (with two to 13 simultaneously recorded units), then it dropped remarkably to an average of two to three detectable single units per animal during the subsequent 3–4 weeks (Figure 6A). Usually, after 5 weeks, the SUA disappeared in most of the animals (Figure 6A). After this period, only one to two single units with smaller spike amplitudes could be detected in three out of six rats. In contrast, MUA could be recorded, at least on some of the channels, until the end of the experiment. The mean and SD of the peak-to-peak amplitude of mean spike waveforms were found to be $113.01 \pm 94.02 \mu\text{V}$ (range: 30–606 μV , $n=481$ single units from nine rats). Usually, new single units appeared during consecutive recording sessions with the parallel

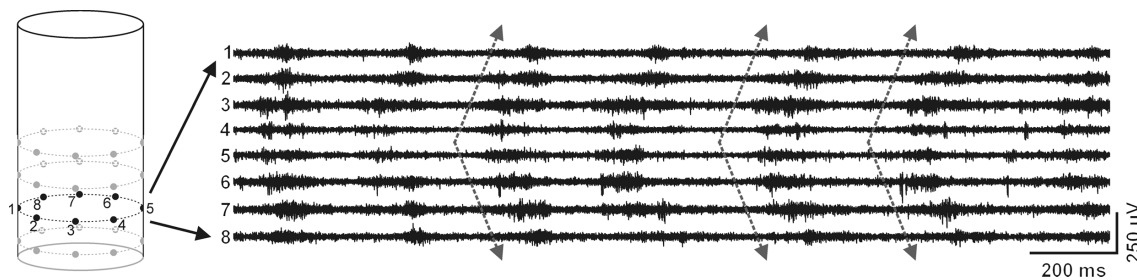


Figure 5: Representative example of the propagation of multi-unit activity (MUA) in the thalamus during ketamine/xylazine-induced slow-wave activity.

Traces on the right show 2-s-long thalamic MUA recorded with eight recording sites of the cylindrical depth probe (left). The electrodes were located at the same depth level. In this example, the MUA started on channel 4 or 5 in most cases and propagated around the circumference of the probe (representative events indicated by gray dashed arrows).

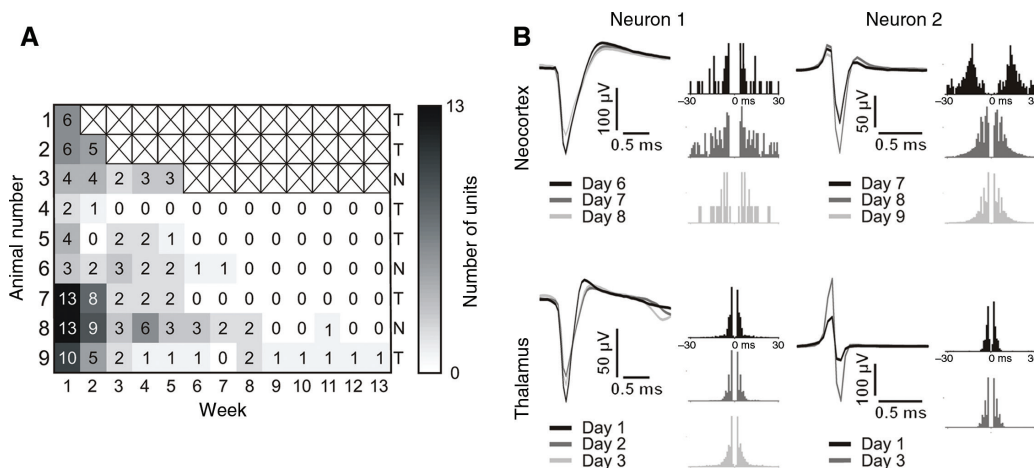


Figure 6: Evaluation of the recorded single-unit activity.

(A) The maximal number of simultaneously recorded single units which could be isolated each week for each animal over time during a single recording session. Animals 1, 2 and 3 were sacrificed after 1, 2 and 5 weeks, respectively. The three probes comprising Pt-nanoglass electrodes were implanted into animals 4, 5 and 8. N, Neocortex; T, thalamus. (B) Mean spike waveforms and autocorrelograms (bin size: 1 ms) of representative single units from the neocortex (top) and the thalamus (bottom) which presumably could be recorded on the same electrode channel for multiple consecutive days. For each neuron, the mean spike waveforms obtained during different days are overlaid. In the case of the last example (bottom right), there was no recording during day 2. The spikes of single units from the neocortex were recorded by Pt-nanoglass electrodes, while the spikes of thalamic units were obtained by regular Pt electrodes.

disappearance of spikes of other neurons. This high turnover rate of single units was likely due to the electrode drift, i.e. micromotions between the implant and the brain tissue. We could, however, identify several neurons whose spikes were detected on the same channel of the probe for several consecutive days (Figure 6B). Such stable units, with only a moderate change in the amplitude of their mean action potential waveform, were observed both in the neocortex and the thalamus. To identify these neurons, we compared the shape of the mean spike waveforms and the autocorrelograms of isolated single units between successive days (Figure 6B).

To further quantify the long-term performance of the cylindrical probe, the grand average SNR was calculated

and the temporal change of the SNR was examined across weeks (Figure 7A). The SNR computed on MUA traces is a commonly used measure to objectively track the recording capabilities of a neural implant over time [22–24]. Unit activity recorded with cylindrical depth probes showed the highest SNR values during the first 2 weeks after the implantation, in accordance with the high single unit yield observed during this period (Figure 7A). During the subsequent weeks, the SNR started to decrease until it reached its minimum after 9 weeks and did not show any noticeable improvement later (Figure 7A). In the case of two experiments (Animal 7 and 8 in Figure 6A), individual channels were also grouped into three categories based on their respective SNR values, to examine the temporal

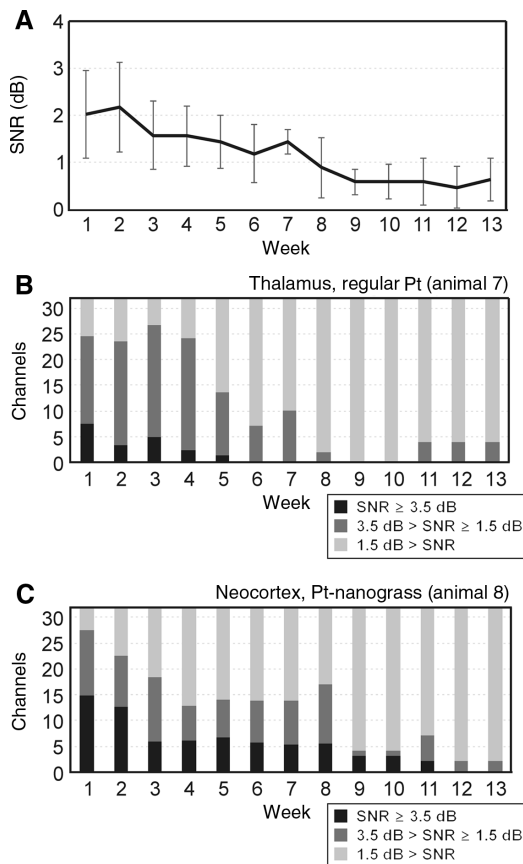


Figure 7: Temporal change of the signal-to-noise ratio (SNR). (A) Change of the grand average SNR over time constructed from data of all animals. (B, C) Temporal change of the distribution of channels with high SNR ($\text{SNR} \geq 3.5$ dB), moderate SNR ($3.5 \text{ dB} > \text{SNR} \geq 1.5 \text{ dB}$) or low SNR ($\text{SNR} < 1.5 \text{ dB}$) in two animals (B, thalamic implantation, animal 7 with regular Pt electrodes; C, neocortical implantation, animal 8 with Pt-nanograss electrodes).

evolution of the number of channels providing useful electrophysiological data (Figure 7B and C). Based on the SNR measurement method used in this study, high SNR (≥ 3.5 dB) might indicate the presence of unit activity comprising separable single units (i.e. SUA), while moderate SNR ($3.5 \text{ dB} > \text{SNR} \geq 1.5 \text{ dB}$) can be measured when spikes with lower amplitudes are detected which are generated by a large population of neurons located farther away from the recording sites (i.e. MUA). Furthermore, low SNR ($< 1.5 \text{ dB}$) is usually a sign of decreased recording performance due to mechanical or biological failure. During the first 2–3 weeks, high or moderate SNR was measured on most of the channels and only a few channels did not show any detectable physiological activity (low SNR). However, after 8 weeks, only a minority of channels were classified in the “high SNR” group, while no action potential firing could be detected on most of the channels (Figure 7B

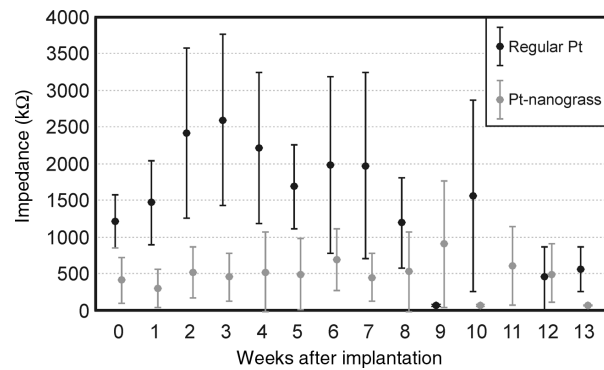


Figure 8: Temporal change of the grand average electrical impedance of recording sites measured at 1 kHz in the brain tissue. Black values correspond to the mean and SD of the impedance of probes with regular Pt electrodes, while gray values indicate the impedance of probes containing Pt-nanograss coated electrodes. On the x-axis, zero corresponds to the day of implantation. In the case of regular Pt electrodes, the impedance measurement was unsuccessful during the 11th week. In a minority of cases very low impedances were measured (regular Pt, week 9; Pt-nanograss, weeks 10 and 13).

and C). In contrast, some channels with moderate SNR were present until the end of the experiments.

To complement the investigations on the electrophysiological data, we also examined the weekly change of the electrical impedance of the recording sites (Figure 8). On the day of implantation, the mean impedance of probes containing Pt-nanograss electrodes was considerably lower compared to the impedance of probes with regular-Pt electrodes ($413 \pm 309 \text{ k}\Omega$ versus $1212 \pm 365 \text{ k}\Omega$, measured at 1 kHz in the brain tissue), and also remained mostly lower until the end of the experiments. Impedance measurements of probes with regular Pt electrodes showed an increase of impedance values during the first few weeks, which corresponds to the time interval in which brain signals could be recorded with good quality. The impedance of regular Pt sites started to decrease noticeably after 8–9 weeks, with a large subset of electrodes showing very low impedances. This reduction of impedance values could be a sign of shorted circuits probably due to material failure. In contrast, the impedance values of Pt-nanograss electrodes were relatively stable during the whole 13 weeks of the experiments (SD of the grand average impedance values: Pt-nanograss, $218 \text{ k}\Omega$; regular Pt, $778 \text{ k}\Omega$). Such stability was expected based on the previously reported electrochemical and mechanical stability of the Pt-nanograss coating *in vitro* [25] and could here be verified also under *in vivo* conditions.

We also examined whether there might be a difference in the single-unit recording capability of the two types of electrode metalizations. First, we measured the RMS noise

level of microelectrodes of probes in physiological saline solution. The probes were placed in the same Faraday cage which was also used during the *in vivo* recordings. We found, that the *in vitro* noise level was slightly lower in the case of Pt-nanograss recording sites ($3.21 \pm 0.36 \mu\text{V}_{\text{rms}}$ versus $4.61 \pm 1.08 \mu\text{V}_{\text{rms}}$, mean \pm SD of eight electrodes of each type). Furthermore, the peak-to-peak amplitudes of the mean spike waveform of single units recorded with cylindrical probes with Pt-nanograss electrodes were significantly higher compared to the amplitudes of spikes obtained with depth probes comprising regular Pt electrodes (Pt-nanograss, mean \pm SD: $185.41 \pm 153.11 \mu\text{V}$, range: 30–606 μV , $n=107$ single units; regular Pt, mean \pm SD: $91.17 \pm 47.73 \mu\text{V}$, range: 32–511 μV , $n=374$ single units; unpaired t-test, $p < 0.001$). Uncorrelated with the noise level and spike amplitude, we could on average separate more single units in animals implanted with probes with regular Pt electrodes (62.33 ± 47.91 versus 35.67 ± 34.59 , mean \pm SD).

Evaluation of histocompatibility

To assess the biocompatibility of the implants, histological sections were stained for neuronal cell bodies (NeuN,

Figure 9A and B) or astroglia (GFAP, Figure 10A and B). From each animal which survived the 13 weeks (6/9 rats) and for each staining, three sections were selected for analysis.

In the case of NeuN staining (Figure 9A–C), stained cell bodies were automatically counted in the 20 regions of interest (ROIs) around the probe track and standardized to the cell density in the outermost ROIs (400–500 μm , see Materials and methods section for details of ROI selection). There were no significant differences in cell density between the 20 ROIs for neither the neocortex (Figure 9D, $n=6$, $p=0.46$) nor the thalamus (Figure 9E, $n=12$, $p=0.31$). The variability of cell densities was largest in the ROI closest to the probe track, which was not surprising, as it was 1) the ROI furthest away from the standardization ROIs; and 2) the smallest of the defined ROIs, which also allows more variability than larger ROIs. Although, on average, no significant cell loss was found next to the implanted probes, on the brain sections of two out of six animals dark bands with a thickness of 200–300 μm could be detected (Figure 9C). These putative lesions located adjacent the probe track are presumably the signs of significant tissue damage created during the implantation of the devices. This theory is supported by the observation

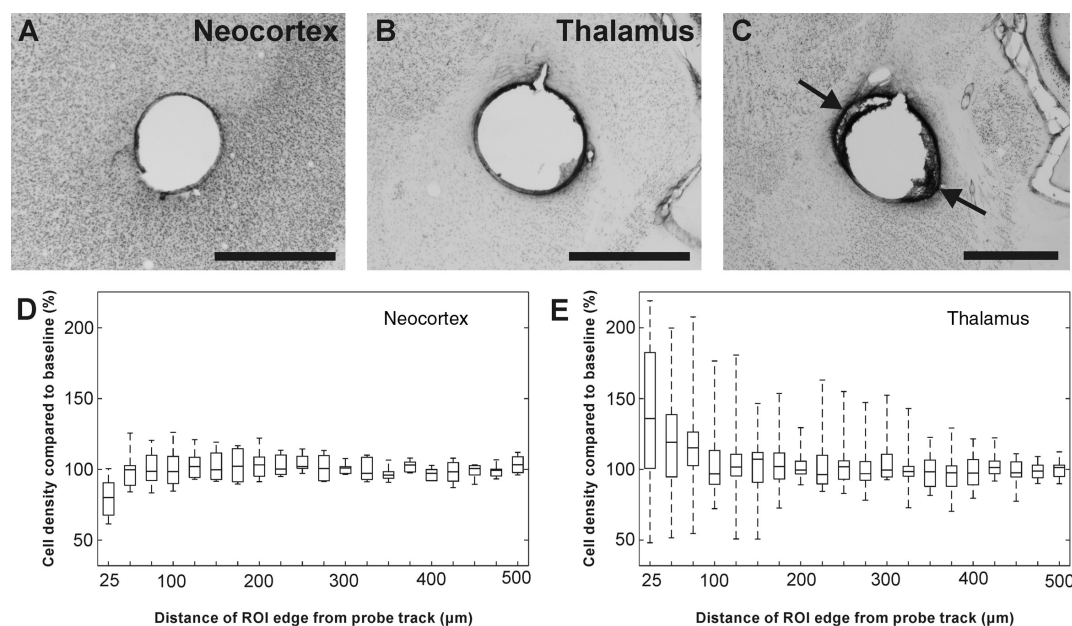


Figure 9: Analysis of NeuN-stained brain sections.

(A, B) Representative brain sections stained for NeuN from the neocortex (A) and the thalamus (B). The white circular hole is the probe track. Small dark dots are stained NeuN. Scale bar: 1 mm. (C) A thalamic brain section containing lesions next to the probe track (dark patches indicated by black arrows). (D, E) Box plots describing cell density across all animals and sections from the neocortex (D) and the thalamus (E) for each of the 20 ROIs (boxes indicate the first and third quantile, whiskers extend to the minimal and maximal values). For each section, the cell density was standardized to the mean of the ROIs from 400 to 500 μm . No significant differences were found between the cell densities of different ROIs.

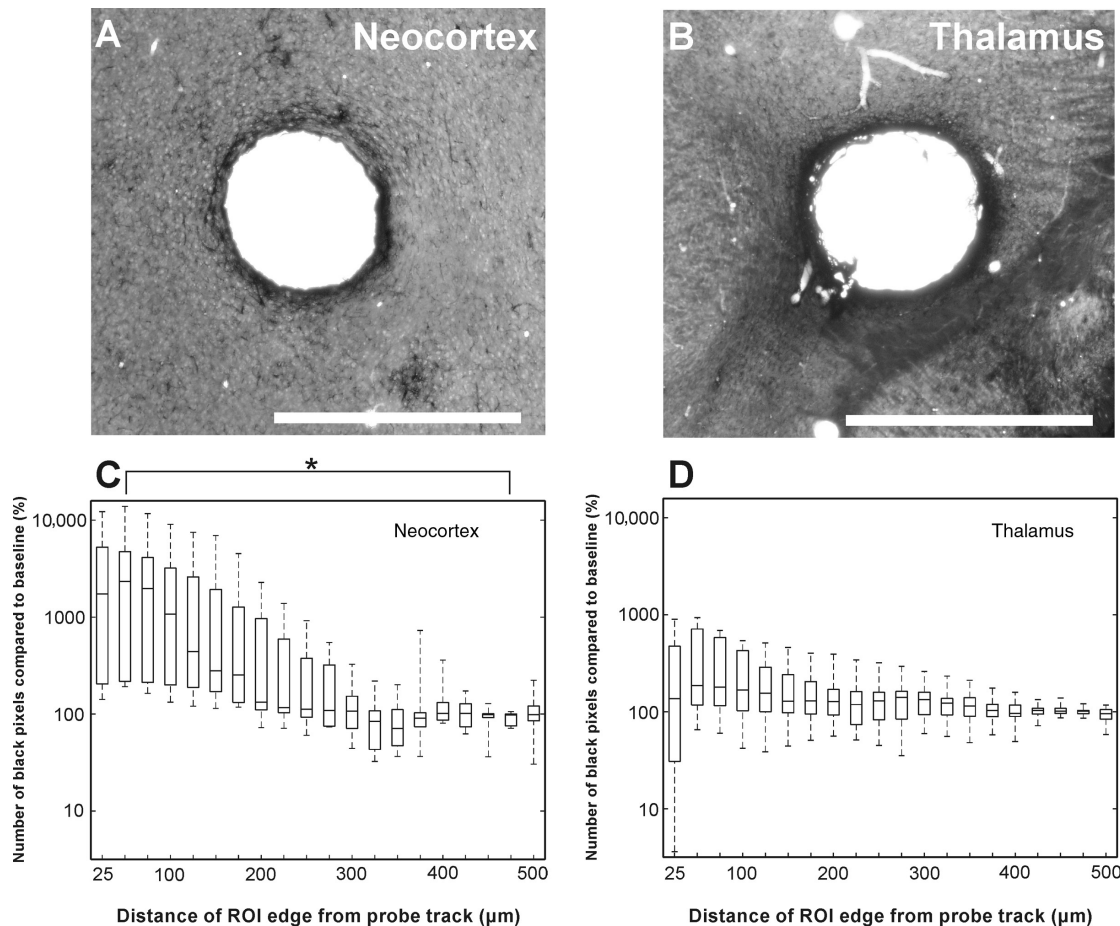


Figure 10: Analysis of GFAP-stained brain sections.

(A, B) Representative brain sections stained for GFAP from the neocortex (A) and the thalamus (B). The white circular hole is the probe track, while the dark, 100-μm-thick band around the track is the glial scar. Scale bar: 1 mm. (C, D) Box plots describing black pixel density across all animals and sections from the neocortex (C) and the thalamus (D) for each of the 20 ROIs (boxes indicate the first and third quantile, whiskers extend to the minimal and maximal values). For each section, the black pixel density was standardized to the mean of the ROIs from 400 to 500 μm. Kruskal-Wallis tests revealed significant differences between the standardized black pixel density for both the neocortex and the thalamus. However, *post-hoc*, the only significant difference between any two groups was between the 25 and 50 μm ROI and the 450–475 micron ROI of the neocortex. * $p < 0.05$.

that among the six animals the single unit yield found during the first days after implantation was the lowest in these two rats (Figure 6A, animals 4 and 5). Furthermore, with the progress of time, SUA also disappeared first in the same two animals.

In the case of GFAP staining (Figure 10A and B), black pixels indicate stained glial cells that form a glial scar around the probe track. The relative mean number of black pixels was highest in the ROIs closest to the probe track in all animals (0–300 μm), both in the neocortex and the thalamus (Figure 10C and D). In case of the neocortex, there was a significant difference between the number of black pixels in the ROIs (Figure 10C, $n = 6$, $p = 1.0597 \times 10^{-6}$), however, the *post-hoc* test only showed significant difference between the second (25–50 μm) ROI and the ROI

before the last (450–475 μm; $p = 0.0461$). The high standardized density of black pixels in ROIs closest to the probe track is caused by the very low number of black pixels in the control ROIs (400–500 μm). In case of the thalamus, there was again a significant difference between the number of black pixels in the ROIs (Figure 10D, $n = 12$, $p = 0.0261$), however, the *post-hoc* test did not show any significant differences between any two groups.

Discussion

In this study, we have presented the *in vivo* characterization of a cylindrical neural interface that is capable of

recording physiological brain activity from the neocortex and thalamus of rats for several weeks.

Electrophysiological performance of the 32-channel cylindrical depth probe

Although, in most of the cases, we could record neuronal signals with good quality shortly after implantation, in several rats unit activity could only be recorded on a small subset of channels or no unit activity could be detected at all. This observation might imply the occurrence of serious tissue damage or bleeding during probe insertion. Considering the large diameter (800 μm) of these neural probes relative to the brain of rodents, this seems a very likely possibility. Signs of significant tissue damage, which were visible on some of the histological sections, also seem to support this theory. Although we used a sharpened wire combined with very slow probe insertion rates to decrease the compression of the tissue, the large-volume probe could still have significantly damaged the brain in a few animals. Though this damage might be serious, it is important to emphasize that these type of probes are primarily intended for the use in humans, which have larger brain sizes than rodents. Furthermore, using more sophisticated implantation strategies may further alleviate the tissue damage during probe insertion (e.g. by avoiding large blood vessels in the brain using two-photon microscopy [26]).

In general, the failure of chronically implanted neural probes is multi-factorial [27]. In our case, the degradation of the recording performance, usually starting 2–3 weeks after implantation, can be partially attributed to the chronic tissue reaction reflected by the loss of neurons and the formation of a glial scar around the probe [10, 11]. However, it had been shown earlier that the damage of the insulating material is also a significant factor in the failure of chronically implanted silicon-based probes, resulting in the degradation of the recording quality or the complete loss of the recording capability of the probe [28, 29]. About 5–6 weeks after implantation, we detected recording sites with very low impedance values on several probes, suggesting the mechanical failure of these electrodes, presumably due to the leakage of extracellular fluids into the device after material failure of the insulation.

During the first 2–3 weeks after implantation, recordings were relatively stable, allowing the simultaneous monitoring of the activity of about a dozen single units at most. The relatively low unit yield obtained with cylindrical depth probes can be attributed to multiple factors. First, the distance between adjacent recording

sites (200 μm vertical and ~ 300 μm horizontal) is too large to record the action potentials of the same neuron on multiple electrodes, which in turn would facilitate the separation of single units, usually resulting in a higher unit yield [30–32]. Furthermore, the extent of tissue damage is proportional to the size of the neural implant [33–35]. Therefore, smaller probes show better recording performance, while larger probes fail to record the activity of many neurons simultaneously. Finally, the breach of the blood-brain barrier during the implantation might also have a significant impact on the long-term recording performance of the probe [36]. Cylindrical probe variants planned for human use will incorporate a higher number of recording sites (128 or more), which will probably increase the single unit yield significantly. Long-term stability of the recorded neurons is also an important factor in chronic studies. The action potential waveforms of some of our recorded neurons were stable for multiple days, similar to the spikes of neurons observed by Okun and colleagues in mice with chronic silicon-based implants [37], as well as cylindrical probes of comparable fabrication technique and size applied in non-human primates [9].

Numerous methods are described in the scientific literature which can be used to decrease the impedance of recording sites and consequently to increase the SNR of neural recordings [12, 38, 39]. Although low-impedance Pt-nanograss recording sites had a lower noise level and recorded single units with higher spike amplitudes, the large variability in the recording performance both across probes and over time makes a quantitative comparison between the two types of electrodes inconclusive. Furthermore, the mean spike amplitude calculated from the data recorded with Pt-nanograss electrodes might be biased by a few high-amplitude single units recorded during the first recording sessions of a single rat. The low number of single units recorded with Pt-nanograss electrodes might be due to the lesions and the higher level of gliosis found on the immunostained brain sections in two out of three animals implanted with probes with this type of coating. Therefore, based on our observations, the conditions of the implantation and the extent of glial scarring may determine the recording properties of the cylindrical probes more significantly than the investigated coatings which in turn will not allow a reliable comparison between the different coatings in this study.

During the first few days after implantation, a similar number of single units could be isolated in the rat data as could be sorted in the monkey data obtained with the earlier 32-channel and 64-channel variants of the cylindrical depth probe [9]. However, in rats, we could record SUA slightly longer (~ 4 weeks in monkey versus ~ 5 weeks in

rats) and we were also able to detect a higher number of single units firing high-amplitude ($>100\text{ }\mu\text{V}$) spikes. The latter observation suggests that more neurons located close to the depth probe survived the implantation procedure, probably due to the use of a slower probe insertion rate ($2\text{--}3\text{ }\mu\text{m/s}$). Furthermore, this study also demonstrated physiologically meaningful neural data obtained from a subcortical structure, the thalamus. This is relevant, in particular, as clinical depth probes for human applications are frequently implanted into brain structures located below the neocortex (e.g. into the subthalamic nucleus targeted in patients with Parkinson's disease). Our findings in thalamic recordings (e.g. propagation of thalamic MUA waves, bursting single units) suggest that cylindrical depth probes are well-suited to record from brain areas other than the neocortex as well.

Biocompatibility of the polyimide depth probe

Based on our examinations, neuronal death was minimal in the $500\text{-}\mu\text{m}$ -thick band around the probe. Occasionally, we found dark lesions with an extent of several hundred microns. These lesions may be the result of serious bleeding or tissue damage caused at the time of probe insertion and not the foreign body response of the brain tissue to the implanted probe, as the single unit yield found during the days after probe insertion was significantly lower in animals with such lesions compared to the unit yield of rats without lesions. This theory is further supported by several studies. For example, lesions caused by the disruption of blood vessels during implantation may significantly affect the recording performance of neural implants [40], since hemorrhagic injury can cause a great degree of cell death [41].

In the neocortex, a moderate cell death could be observed $25\text{ }\mu\text{m}$ from the probe track while cell densities further away were similar to the cell density measured in the control area. In contrast, in the thalamus, the density of neurons was usually higher in the $100\text{-}\mu\text{m}$ -thick band closest to the probe track compared to the control neuron density. A possible explanation for this is that the implanted cylindrical probe, which has a relatively large diameter, compresses the brain tissue around itself and, consequently, neurons will be located closer to each other in the vicinity of the probe, increasing the density of cells. We have two possible theories why this phenomenon could not be observed in neocortex. First, neocortical neurons might be more sensitive to foreign bodies, thus the cell loss in this brain area might be higher compared

to the cell loss in the thalamus. Second, as a small piece of skull was removed above the implantation area, the superficial brain tissue (including the neocortex) may have more space for expansion compared to brain tissue in deeper areas (e.g. the thalamus). However, the higher glial reaction found in cortical sections suggests that both assumptions may be valid and their combined effect might account for the observed differences in the cell density between the two brain structures.

After 3 months, the thickness of the glial scar was found usually around $100\text{--}200\text{ }\mu\text{m}$. A glial sheath with such a thickness prevents the recording of the spikes of nearby neurons which are the main participants of the recorded SUA [10]. This observation was also supported by the acquired electrophysiological data, that is, no SUA could be recorded in most of the animals after 3 months. Furthermore, in animals, where the glial scar was found to be thicker, the single unit yield was usually lower and the spikes of units disappeared earlier as well. Although, in general, SUA could be recorded for $2\text{--}3$ weeks after probe implantation, which is beyond the time needed to detect the epileptic focus in drug resistant patients (~ 10 days), this time period might be further increased by decreasing the foreign body response of the tissue by using untethered electrodes instead of probes tethered to the skull as done in this study [42, 43].

It is further worth mentioning that in comparison to the tissue damage caused by the insertion of the probe itself, the Pt-nanograss coating is here not expected to contribute to increased tissue reactivity since the coating itself only represents a minor fraction of the entire probe surface and has furthermore been shown to exhibit exceptional mechanical stability [25].

As a conclusion, the results of the electrophysiological and histological evaluation demonstrated in this paper provide a strong indication that similar depth probes realized using the fabrication methods described here might be potential candidates to be applied in stereo-electroencephalography recordings and to record human brain electrical activity with increased spatial resolution as well as to provide high single unit yield.

Acknowledgments: The authors wish to thank Ms. E. Szabó-Együd for her help during histological procedures and Mr. P. Kottra for his excellent technical assistance. We are grateful to L. Papp (Neuronelektród Kft.) for the fabrication of the sharpened stainless steel wires.

Author Statement

Research funding: The research leading to these results has received funding from the European Union's Seventh

Framework Programme (FP7/2007–2013) under grant agreement no. 600925 (NeuroSeeker), the Hungarian Brain Research Program Grants (Grant Nos. KTIA_13_NAP-A-I/1, KTIA-13-NAP-A-IV/1-4,6 and 2017-1.2.1-NKP-2017-00002) and was supported by BrainLinks-BrainTools, Cluster of Excellence funded by the German Research Foundation (DFG, grant number EXC 1086). The research within project No. VEKOP-2.3.2-16-2017-00013 by I. Ulbert and D. Horváth was supported by the European Union and the State of Hungary, co-financed by the European Regional Development Fund. R. Fiáth and K. Tóth have received funding from the Hungarian National Research, Development and Innovation Office (Grant Nos. PD124175 and PD121123).

Conflict of interest: The authors declare no conflict of interests.

References

- [1] Engel AK, Moll CK, Fried I, Ojemann GA. Invasive recordings from the human brain: clinical insights and beyond. *Nat Rev Neurosci* 2005;6:35–47.
- [2] Alvarado-Rojas C, Lehongre K, Bagdasaryan J, Bragin A, Staba R, Engel J Jr, et al. Single-unit activities during epileptic discharges in the human hippocampal formation. *Front Comput Neurosci* 2013;7:140.
- [3] Worrell GA, Gardner AB, Stead SM, Hu S, Goerss S, Cascino GJ, et al. High-frequency oscillations in human temporal lobe: simultaneous microwire and clinical macroelectrode recordings. *Brain* 2008;131:928–37.
- [4] Misra A, Burke JF, Ramayya AG, Jacobs J, Sperling MR, Moxon KA, et al. Methods for implantation of micro-wire bundles and optimization of single/multi-unit recordings from human mesial temporal lobe. *J Neural Eng* 2014;11:026013.
- [5] Avanzini P, Abdollahi RO, Sartori I, Caruana F, Pelliccia V, Casaceli G, et al. Four-dimensional maps of the human somatosensory system. *Proc Natl Acad Sci USA* 2016;113:E1936–43.
- [6] Heftt S, Brandt A, Zwick S, von Elverfeldt D, Mader I, Cordeiro J, et al. Safety of hybrid electrodes for single-neuron recordings in humans. *Neurosurgery* 2013;73:78–85; discussion 85.
- [7] Mormann F, Kornblith S, Cerf M, Ison MJ, Kraskov A, Tran M, et al. Scene-selective coding by single neurons in the human parahippocampal cortex. *Proc Natl Acad Sci USA* 2017;114:1153–8.
- [8] Pothof F, Anees S, Leupold J, Bonini L, Paul O, Orban GA, et al. Fabrication and characterization of a high-resolution neural probe for stereoelectroencephalography and single neuron recording. *Conf Proc IEEE Eng Med Biol Soc* 2014;2014:5244–7.
- [9] Pothof F, Bonini L, Lanzilotto M, Livi A, Fogassi L, Orban GA, et al. Chronic neural probe for simultaneous recording of single-unit, multi-unit, and local field potential activity from multiple brain sites. *J Neural Eng* 2016;13:046006.
- [10] Polikov VS, Tresco PA, Reichert WM. Response of brain tissue to chronically implanted neural electrodes. *J Neurosci Methods* 2005;148:1–18.
- [11] Kozai TD, Jaquins-Gerstl AS, Vazquez AL, Michael AC, Cui XT. Brain tissue responses to neural implants impact signal sensitivity and intervention strategies. *ACS Chem Neurosci* 2015;6:48–67.
- [12] Boehler C, Stieglitz T, Asplund M. Nanostructured platinum grass enables superior impedance reduction for neural micro-electrodes. *Biomaterials* 2015;67:346–53.
- [13] Paxinos G, Watson C. *The Rat Brain in Stereotaxic Coordinates*. 6th ed. San Diego: Academic Press/Elsevier; 2007.
- [14] Fiath R, Beregszaszi P, Horvath D, Wittner L, Aarts AA, Ruther P, et al. Large-scale recording of thalamocortical circuits: in vivo electrophysiology with the two-dimensional electronic depth control silicon probe. *J Neurophysiol* 2016;116:2312–30.
- [15] Csicsvari J, Hirase H, Czurko A, Buzsaki G. Reliability and state dependence of pyramidal cell-interneuron synapses in the hippocampus: an ensemble approach in the behaving rat. *Neuron* 1998;21:179–89.
- [16] Hazan L, Zugaro M, Buzsaki G. Klusters, NeuroScope, NDManager: a free software suite for neurophysiological data processing and visualization. *J Neurosci Methods* 2006;155:207–16.
- [17] Seidl K, Torfs T, De Maziere PA, Van Dijk G, Csicsvari R, Dombvari B, et al. Control and data acquisition software for high-density CMOS-based microprobe arrays implementing electronic depth control. *Biomed Tech (Berl)* 2010;55:183–91.
- [18] Schneider CA, Rasband WS, Eliceiri KW. NIH Image to ImageJ: 25 years of image analysis. *Nat Methods* 2012;9:671–5.
- [19] Schindelin J, Arganda-Carreras I, Frise E, Kaynig V, Longair M, Pietzsch T, et al. Fiji: an open-source platform for biological-image analysis. *Nat Methods* 2012;9:676–82.
- [20] Fiath R, Kerekes BP, Wittner L, Toth K, Beregszaszi P, Horvath D, et al. Laminar analysis of the slow wave activity in the somatosensory cortex of anesthetized rats. *Eur J Neurosci* 2016;44:1935–51.
- [21] Slezia A, Hangya B, Ulbert I, Acsady L. Phase advancement and nucleus-specific timing of thalamocortical activity during slow cortical oscillation. *J Neurosci* 2011;31:607–17.
- [22] Vetter RJ, Williams JC, Hetke JF, Nunamaker EA, Kipke DR. Chronic neural recording using silicon-substrate microelectrode arrays implanted in cerebral cortex. *IEEE Trans Biomed Eng* 2004;51:896–904.
- [23] Han M, Manoonkitiwongsa PS, Wang CX, McCreery DB. In vivo validation of custom-designed silicon-based microelectrode arrays for long-term neural recording and stimulation. *IEEE Trans Biomed Eng* 2012;59:346–54.
- [24] Patel PR, Zhang H, Robbins MT, Nofar JB, Marshall SP, Kobylarek MJ, et al. Chronic in vivo stability assessment of carbon fiber microelectrode arrays. *J Neural Eng* 2016;13:066002.
- [25] Boehler C, Oberueber F, Stieglitz T, Asplund M. Nanostructured platinum as an electrochemically and mechanically stable electrode coating. In: 39th annual international conference of the IEEE Engineering in Medicine and Biology Society (EMBC), Seogwipo, South Korea, July 11–15, 2017. Piscataway, NJ: IEEE; 2017:1058–61.
- [26] Kozai TD, Marzullo TC, Hooi F, Langhals NB, Majewska AK, Brown EB, et al. Reduction of neurovascular damage resulting from microelectrode insertion into the cerebral cortex using in vivo two-photon mapping. *J Neural Eng* 2010;7:046011.

- [27] Prasad A, Xue QS, Sankar V, Nishida T, Shaw G, Streit WJ, et al. Comprehensive characterization and failure modes of tungsten microwire arrays in chronic neural implants. *J Neural Eng* 2012;9:056015.
- [28] Barrese JC, Rao N, Paroo K, Triebwasser C, Vargas-Irwin C, Franquemont L, et al. Failure mode analysis of silicon-based intracortical microelectrode arrays in non-human primates. *J Neural Eng* 2013;10:066014.
- [29] Kozai TD, Catt K, Li X, Gugel ZV, Olafsson VT, Vazquez AL, et al. Mechanical failure modes of chronically implanted planar silicon-based neural probes for laminar recording. *Biomaterials* 2015;37:25–39.
- [30] Gray CM, Maldonado PE, Wilson M, McNaughton B. Tetrodes markedly improve the reliability and yield of multiple single-unit isolation from multi-unit recordings in cat striate cortex. *J Neurosci Methods* 1995;63:43–54.
- [31] Harris KD, Henze DA, Csicsvari J, Hirase H, Buzsaki G. Accuracy of tetrode spike separation as determined by simultaneous intracellular and extracellular measurements. *J Neurophysiol* 2000;84:401–14.
- [32] Rey HG, Pedreira C, Quiroga RQ. Past, present and future of spike sorting techniques. *Brain Res Bull* 2015;119:106–17.
- [33] Karumbaiah L, Saxena T, Carlson D, Patil K, Patkar R, Gaupp EA, et al. Relationship between intracortical electrode design and chronic recording function. *Biomaterials* 2013;34:8061–74.
- [34] Kozai TD, Langhals NB, Patel PR, Deng X, Zhang H, Smith KL, et al. Ultrasmall implantable composite microelectrodes with bioactive surfaces for chronic neural interfaces. *Nat Mater* 2012;11:1065–73.
- [35] Seymour JP, Kipke DR. Neural probe design for reduced tissue encapsulation in CNS. *Biomaterials* 2007;28:3594–607.
- [36] Saxena T, Karumbaiah L, Gaupp EA, Patkar R, Patil K, Betancur M, et al. The impact of chronic blood-brain barrier breach on intracortical electrode function. *Biomaterials* 2013;34:4703–13.
- [37] Okun M, Lak A, Carandini M, Harris KD. Long term recordings with immobile silicon probes in the mouse cortex. *PLoS One* 2016;11:e0151180.
- [38] Ludwig KA, Langhals NB, Joseph MD, Richardson-Burns SM, Hendricks JL, Kipke DR. Poly(3,4-ethylenedioxythiophene) (PEDOT) polymer coatings facilitate smaller neural recording electrodes. *J Neural Eng* 2011;8:014001.
- [39] Marton G, Bakos I, Fekete Z, Ulbert I, Pongracz A. Durability of high surface area platinum deposits on microelectrode arrays for acute neural recordings. *J Mater Sci Mater Med* 2014;25:931–40.
- [40] Nolte NF, Christensen MB, Crane PD, Skousen JL, Tresco PA. BBB leakage, astrogliosis, and tissue loss correlate with silicon microelectrode array recording performance. *Biomaterials* 2015;53:753–62.
- [41] Xue M, Del Bigio MR. Intracortical hemorrhage injury in rats: relationship between blood fractions and brain cell death. *Stroke* 2000;31:1721–7.
- [42] Biran R, Martin DC, Tresco PA. The brain tissue response to implanted silicon microelectrode arrays is increased when the device is tethered to the skull. *J Biomed Mater Res A* 2007;82:169–78.
- [43] Ersen A, Elkabes S, Freedman DS, Sahin M. Chronic tissue response to untethered microelectrode implants in the rat brain and spinal cord. *J Neural Eng* 2015;12:016019.